Int. J. Electrochem. Sci., 11 **(2016)** 4310 – 4322, doi: 1020964/2016.06.69

International Journal of ELECTROCHEMICAL SCIENCE
www.electrochemsci.org

Comparative Studies on MG49-$LiClO_4$ and MG49-TiO_2-SiO_2-$LiClO_4$ Polymer Electrolytes

Oon Lee Kang[1,3], *Azizan Ahmad*[1,*], *Nur Hasyareeda Hassan*[1,*], *Usman Ali Rana*[2], *Claudio Migliaresi*[3]

[1] Faculty Science and Technology, Universiti Kebangsaan Malaysia, 43600 Bangi, Selangor, Malaysia
[2] Sustainable Energy Technologies Center, King Saud University, P.O. Box 800, Riyadh 11421, Saudi Arabia
[3] Biotech Research Center, Universita di Trento, via delle Regole 101, 38123 Mattarello, Trento, Italy
[*]E-mail: azizan@ukm.my; syareeda@ukm.edu.my

Received: 14 October 2015 / *Accepted:* 23 March 2016 / *Published:* 4 May 2016

MG49-$LiClO_4$ and MG49-TiO_2-SiO_2-$LiClO_4$ polymer electrolytes were prepared through solution-cast technique. In the present case, MG49-$LiClO_4$ and MG49-TiO_2-SiO_2-$LiClO_4$ polymer electrolytes were subjected to structural, electrochemical, and some other relevant analyses. MG49-$LiClO_4$ and MG49-TiO_2-SiO_2-$LiClO_4$ polymer electrolytes had exhibited hierarchical structure changes upon different salt-loaded levels. MG49-$LiClO_4$ and MG49-TiO_2-SiO_2-$LiClO_4$ polymer electrolytes had achieved maximum ionic conductivities at 25 wt.% salt-loaded level. In comparison, MG49-$LiClO_4$ and MG49-TiO_2-SiO_2-$LiClO_4$ polymer electrolytes had demonstrated distinct transport mechanisms in a similar experimental configuration. MG49-$LiClO_4$ and MG49-TiO_2-SiO_2-$LiClO_4$ polymer electrolytes had exhibited different stability characteristics over a certain operational range.

Keywords: Polymer electrolyte; Sol-gel method; Solution-cast technique

1. INTRODUCTION

Solid polymer electrolytes (SPEs) are attractive alternative to conventional liquid electrolytes [1]. PEO-LiX polymer electrolytes were first introduced in the early 1970s; and then, subsequent research efforts are dedicated to performance improvement [2, 3]. To date, most research studies have focused on three core aspects: fundamental science (e.g. structural characteristics, electrochemical stabilities and dielectric properties); mechanistic basis; and technological innovation [4, 5].

SPEs are more compliant than ever before [6]. Such predominant is attributed to several characteristic properties: simple fabrication procedure; flexible geometric construction; and stable operational system [7, 8]. SPEs have shown tremendous potential in numerous technological devices. SPEs are critical component in diverse electrochemical applications [9].

In practice, SPEs should achieve adequate ionic conductivities (~ 10^{-4} S/cm) at ambient temperature [10, 11]. In most cases, however, SPEs does not exhibit appreciable ionic conductivities (< 10^{-8} S/cm) at ambient temperature [12]. SPEs might lose ionic conductivities upon unfavorable conditions: crystalline structure inherent; simultaneous ionic motion; and transient ionic interaction [13].

Nanocomposite polymer electrolytes (NPEs) are breakthrough to innovative electrochemical technology. NPEs are often obtained through reinforcement strategies: electrostatic stabilization; covalent immobilization; and non-covalent immobilization [14]. NPEs can achieve high ionic conductivities through alternative pathways [15].

NPEs are considered as heterogeneous system [16]. Ionic transport is quite complicated in heterogeneous system. Ionic transport is relied on multiple interactive factors [17]. In general, ionic transport is facilitated through segmental relaxation. In addition, ionic transport is mediated through lattice dislocation.

In the present investigation, MG49-$LiClO_4$ and MG49-TiO_2-SiO_2-$LiClO_4$ polymer electrolytes were prepared through solution-cast technique. MG49-$LiClO_4$ and MG49-TiO_2-SiO_2-$LiClO_4$ polymer electrolytes were further subjected to structural, electrochemical, and some other relevant analyses.

2. EXPERIMENT

2.1 Polymer Electrolyte Preparation

MG49-$LiClO_4$ polymer electrolytes were fabricated through simple solution-cast techniques. $LiClO_4$ salt solutions were prepared at different concentration ratios; and then introduced into preformed MG49 polymer host matrices. Resultant mixture solutions were stirred overnight at ambient temperature; and then cast into Teflon petri dishes. Resultant thin films were further dried in vacuum oven.

MG49-TiO_2-SiO_2-$LiClO_4$ polymer electrolytes were fabricated through combination sol-gel and solution-cast techniques. TiO_2-SiO_2 sol particles were first prepared through HNO_3/EtOH catalysis; and then introduced into preformed MG49-$LiClO_4$ polymer electrolyte matrices. Resultant mixture solutions were stirred ½ hours at ambient temperature; and then cast into Teflon petri dishes. Resultant thin films were further dried in vacuum oven.

2.2 Polymer Electrolyte Characterization

XRD analyses were conducted on a Bruker D8 Advance diffractometer (Bruker, Germany). XRD analyses were performed at the CuKα radiation wavelength. XRD patterns were acquired in a Bragg-Brentano configuration. XRD patterns were recorded in the 2-theta range (15 - 60°; step size 0.02°).

FTIR analyses were conducted on a Perkin-Elmer Spectrum 400 spectrometer (Perkin Elmer, United Kingdom). FTIR spectra were acquired in the attenuated total reflectance (ATR) mode. FTIR spectra were recorded in the mid infrared range (4000 - 650 cm^{-1}; spectral resolution 4 cm^{-1}).

EIS analyses were conducted on a Solartron Schlumberger SI 1286 potentiostat (Solartron Schlumberger, Farnborough, England). EIS spectra were acquired in the alternative current (AC) modulation. Impedance spectra were recorded in the medium frequencies region (1 Hz – 1 kHz).

SEM analyses were conducted on a LEO 1450 VP instrument (Carl Zeiss, Oberkochen, Germany). SEM analyses were performed at a low acceleration voltage. SEM images were acquired in the backscattered electrons mode. SEM images were taken at a high magnification.

TGA analyses were conducted on a Shimadzu TGA-50 instrument (Shimadzu, Japan). TGA scans were recorded in a broad temperature range (room temperature to 600 °C; scan rate 10°C min^{-1}).

DRA analyses were conducted on Anton Paar Physica MCR 501 rheometer (Anton Paar, Austria). DRA analyses were performed at isothermal condition. DRA responses were acquired in a dynamic oscillation mode.

3. RESULT AND DISCUSSION

3.1 Structural Studies

Broad humps were observed in MG49 diffraction pattern. Such humps are attributed to semicrystalline structure. In this case, soft segment is attributed to isoprene chain; meanwhile, hard segment is attributed to PMMA grafted onto rubber chain.

Small humps were observed in MG49-TiO_2-SiO_2 diffraction pattern. In this case, therefore, amorphous structure is dominant in MG49-TiO_2-SiO_2 polymer composite. Such phenomenon is attributed to particle-polymer interaction [7]. Local chain reorganization is inhibited upon particle-polymer interaction.

Characteristic broad hump (2θ = 15°) had become flattened upon lithium salt insertion. Such phenomenon is attributed to chain destruction. Broad amorphous hump had shifted to high 2-theta angles. Such phenomenon is attributed to lattice distortion.

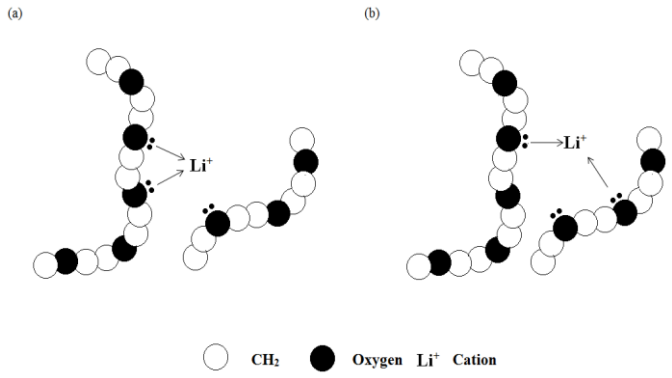

Figure 1. Lithium cation solvation (a) intrachain and (b) interchain

$LiClO_4$ recrystallization does take place at high salt concentration. $LiClO_4$ characteristic diffraction peaks had become more apparent at 2θ = 21.1, 23.3, 31.7, 33.1 and 35.7°. $LiClO_4$ characteristic diffraction peaks had become less intense in MG49-TiO_2-SiO_2-$LiClO_4$ diffraction

patterns. In such a case, Li^+ cation solvation is further enhanced upon TiO_2-SiO_2 reinforcement. Such phenomenon is attributed to dielectric improvement. Li^+ cation solvation are mediated through cation-polymer interaction (Figure 1).

TiO_2-SiO_2 diffraction lines did not detected in MG49-TiO_2-SiO_2 diffraction pattern. TiO_2-SiO_2 crystalline fraction is much less than several percentages. Such phenomenon is attributed to unstable equilibrium state. Sol-gel reaction is driven in unstable thermodynamic condition.

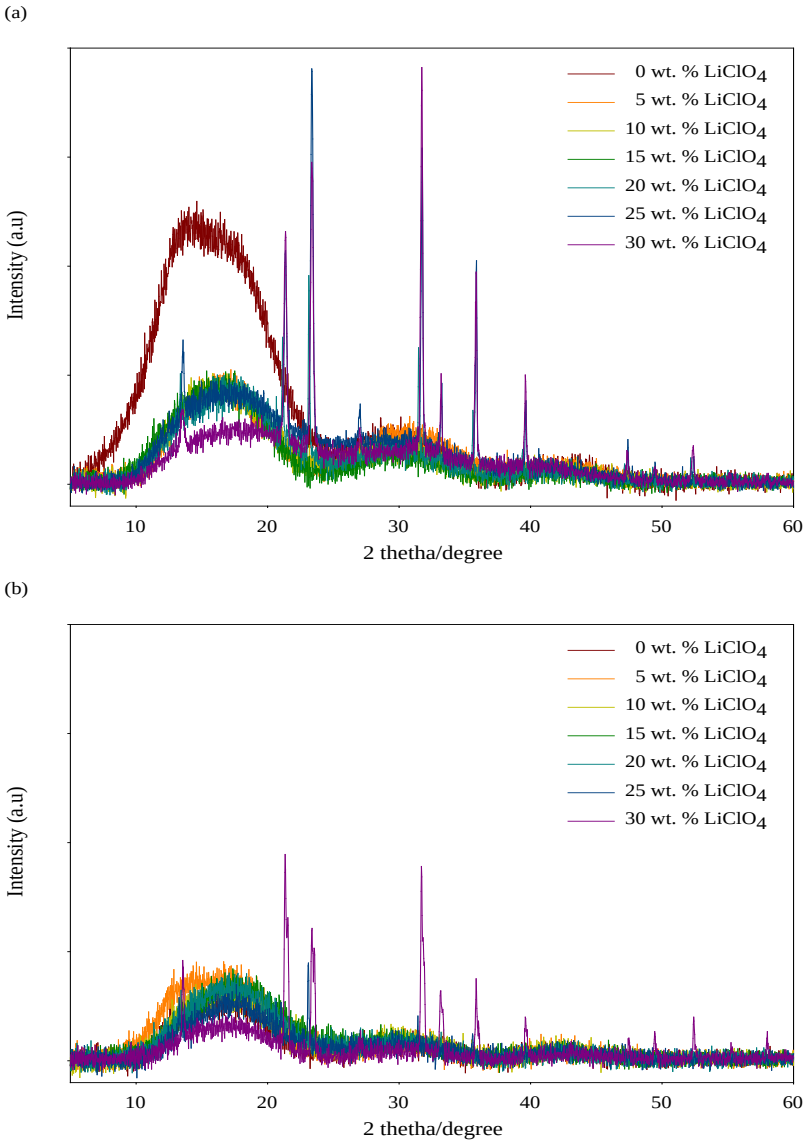

Figure 2. Diffraction patterns (a) MG49-$LiClO_4$ and (b) MG49-TiO_2-SiO_2-$LiClO_4$ polymer electrolyte

Infrared spectra are depicted in Figure 3. Special attention is focused on electron donor atoms (Figure 4). Polymer/Li^+ complexation does take place on ether oxygen chains. Polymer/Li^+ complexation can lead to dramatic frequency changes. Major absorption features is identified in these vibrational regions: 3400 - 3600 cm^{-1} (-OH stretch), 2960 - 2860 cm^{-1} (-CH_3 stretch), 1750 - 1730 cm^{-1} (C=O stretch) and 1250 - 950 cm^{-1} (C-O-C stretch).

Hydroxyl absorption band did not appear in MG49 spectra. Such absorption band had become apparent upon lithium salt insertion. Hydroxyl absorption band had evolved into two distinct peaks. Such phenomenon is attributed to intramolecular bond formation.

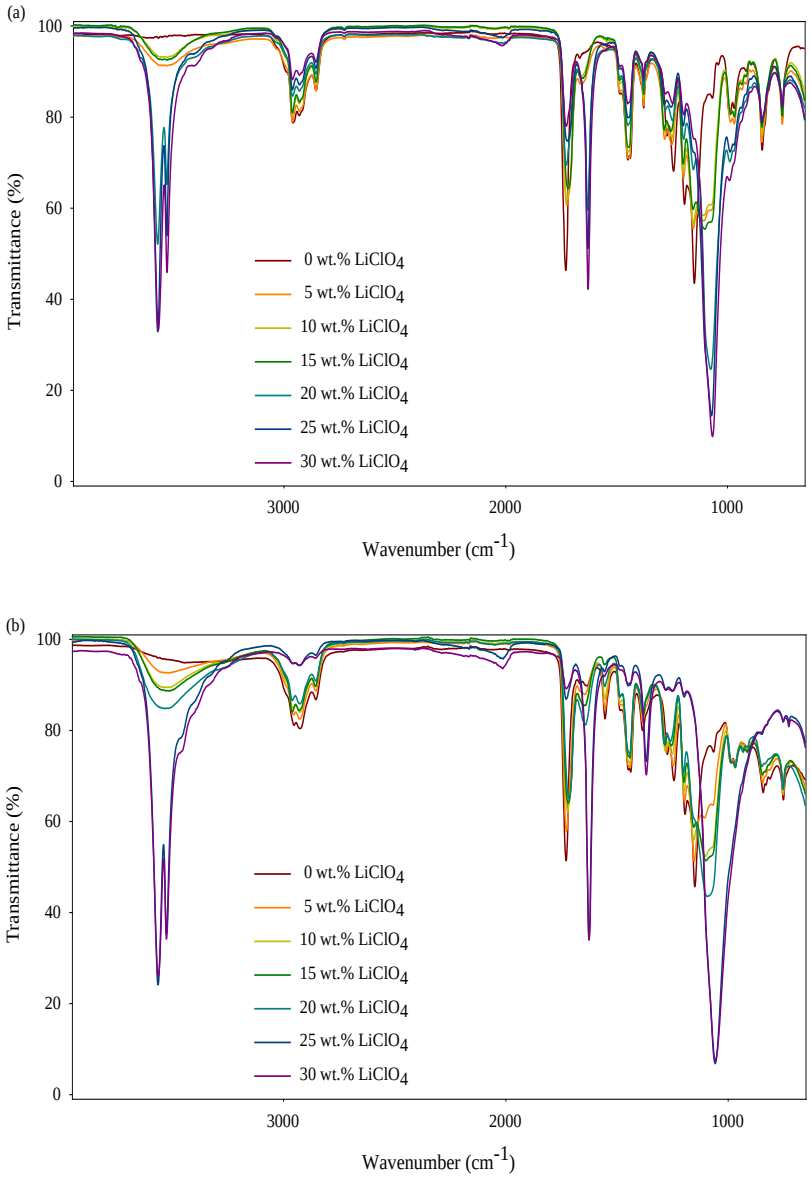

Figure 3. FTIR absorption spectra (a) MG49-$LiClO_4$ and (b) MG49-TiO_2-SiO_2-$LiClO_4$ polymer electrolyte

Carbonyl v(C=O) absorption band had become broadened upon lithium salt insertion. Such phenomenon is attributed to coordinate bond formation [18].

Ether (C-O-C) absorption bands had detected at different vibrational modes: v(C-O), v_s(C-O-C), v_{as}(C-O-C) and δ(O-CH_3) (Figure 4). COO^- absorption band is shifted upward upon lithium salt insertion. δ(O-CH_3) absorption band had remained unchanged upon lithium salt insertion.

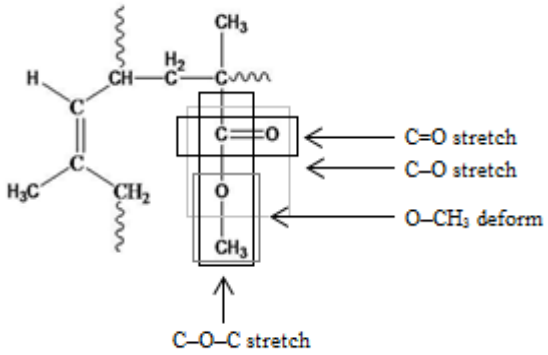

Figure 4. MG monomeric structure

$LiClO_4$ recrystallization does take place at high salt concentration. $LiClO_4$ characteristic absorption bands had become apparent at 1630 and 1065 cm^{-1}. $LiClO_4$ recrystallization is attributed to ionic association.

3.2 Electrochemical Studies

Ionic conductivities were investigated through electrochemical impedance spectroscopic measurements. Ionic conductivities are controlled through multiple parameters: $\sigma = pq\mu$. In effect, ionic conductivities are proportional to total ionic mobilities [19]. Ionic conductivities are presented in Table 1. Ionic conductivities are obtained through the relationship:

$$\sigma = \frac{1}{\text{Bulk resistance}} \times \frac{\text{Membran thickness}}{\text{Electrode area}}$$

Single capacitive semicircle was observed in high frequency region. Such capacitive semicircle is implicated to bulk properties. In general, single capacitive semicircle is characterized as parallel resistor-capacitor circuits [20]. Steep spike was observed in low frequency region. Steep spike is correlated to electrode polarization effect. In fact, steep spike is attributed to high charge carrier accumulation [21]. Fast ion dynamic can lead to high charge carrier accumulation.

Table 1. Concentration-dependence ionic conductivities

x wt. % $LiClO_4$	Ionic conductivity (S/cm)	
	MG49-$LiClO_4$	MG49-TiO_2-SiO_2-$LiClO_4$
0	7.14×10^{-11}	1.13×10^{-11}
5	2.49×10^{-10}	1.03×10^{-11}
10	4.02×10^{-10}	1.01×10^{-11}
15	1.48×10^{-09}	3.61×10^{-10}
20	1.94×10^{-08}	2.46×10^{-08}
25	3.20×10^{-08}	6.95×10^{-07}
30	7.51×10^{-09}	9.54×10^{-09}

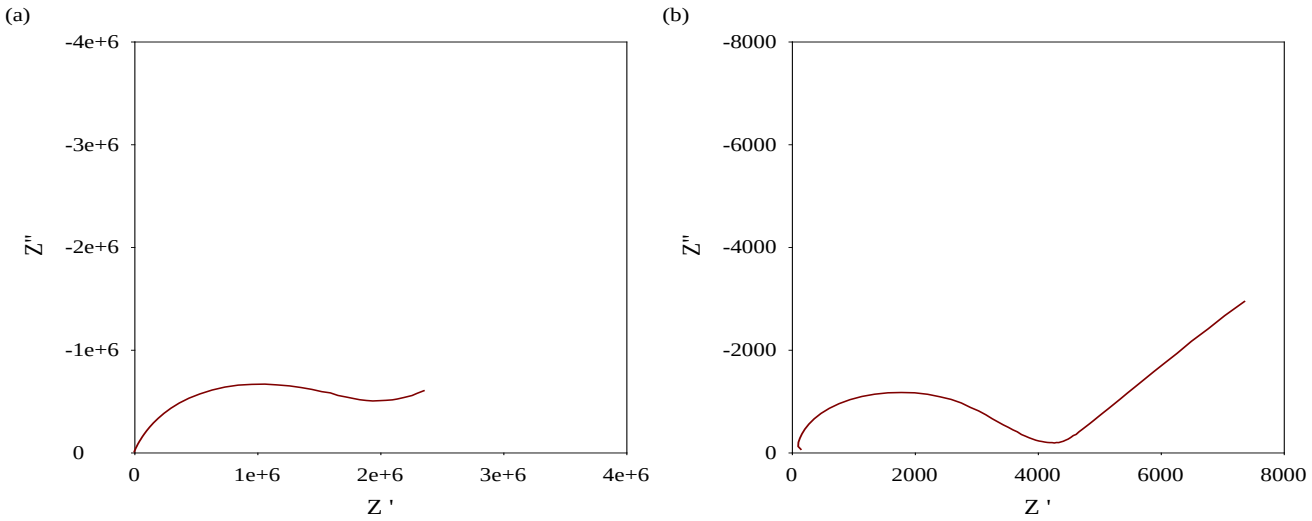

Figure 5. Complex impedance plots (a) MG49-25 wt.% $LiClO_4$ and (b) MG49-TiO_2-SiO_2-25 wt.% $LiClO_4$ polymer electrolyte

Ionic conductivities had increased upon lithium salt insertion. Such phenomenon is attributed to free charge carrier increment. Polymer/Li^+ complexation is much more apparent upon free charge carrier increment [22]. Maximum ionic conductivities had attained at 25 wt. % salt insertion. Such phenomenon is attributed to maximum O-Li^+ interaction. Local segmental movement is mediated through significant O-Li^+ interaction.

$$LiClO_4(s) \rightarrow Li^+(aq) + ClO_4^-(aq) \quad (1)$$

$$Li^+(aq) + ClO_4^-(aq) + -[MG49]_n - (aq) \rightarrow ClO_4^- - [MG49_n] - Li^+ \quad (2)$$

Ionic conductivities had reduced at high salt concentration. Such phenomenon is attributed to ionic association. Ionic cluster formation is favored at high salt concentration. Ionic cluster formation is attributed to coulomb interaction. In effect, mobile charge carrier is less available in ionic conduction. In addition, dielectric constant is diminished to some extent. Transient crosslink network formation is favored at high salt concentration. In consequence, local segmental motion is constrained to some extent [22]. Similar trends were observed in several previous studies [23].

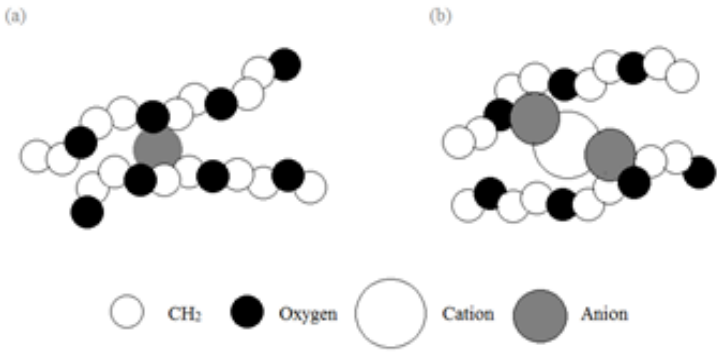

Figure 6. Transient crosslink networks (a) cation-cation interaction and (b) cation-anion interaction

Ionic conductivities were much greater in MG49-TiO_2-SiO_2-$LiClO_4$ polymer electrolyte. Ionic conductivities are further enhanced upon TiO_2-SiO_2 reinforcement. Such phenomenon is attributed to Lewis acid-base interaction. Bulk resistivity is reduced upon particle-polymer interaction. In general, bulk resistance is determined through low frequency x-intercept.

Ionic conductivities had increased upon temperature increment. Such phenomenon is attributed to several factors: high salt dissociation; rapid segmental movement; and large free volume. Log σ-1000/T plot is not linear but polynomial. In such a case, distinct behavior is revealed in the entire temperature range. Distinct behavior is attributed to structural phase transition [23, 24]. Arrhenius behavior is exhibited at low temperature region. Arrhenius conduction is regulated through lattice diffusion, i.e. substitutional diffusion and/or indirect interstitial diffusion [25]. VTF behavior is exhibited at high temperature region. VTF conduction is regulated through segmental relaxation [26].

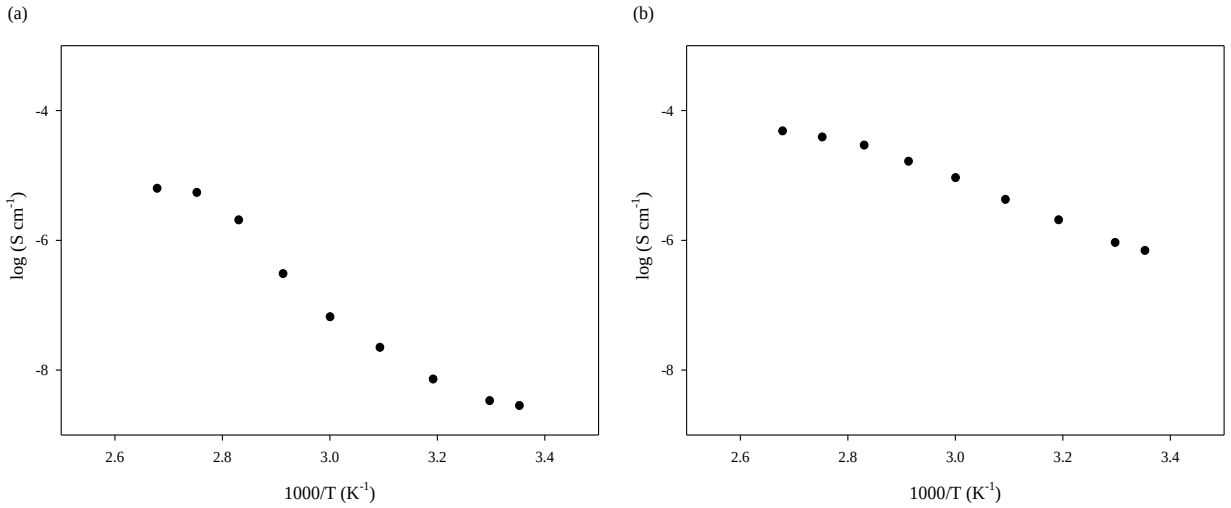

Figure 7. Temperature-dependence ionic conductivities (a) MG49-25 wt.% $LiClO_4$ and (b) MG49-TiO_2-SiO_2-25 wt.% $LiClO_4$ polymer electrolyte

Log σ-1000/T plot is much different in MG49-TiO_2-SiO_2-25 wt.% $LiClO_4$ polymer electrolyte. Distinct behavior is exhibited at the defect region. Ionic conduction is coupled to grain boundary diffusion.

Quasi-rectangular shape was observed in fast-scan cyclic voltammograms. Such feature is denoted as ideal electrochemical capacitive behavior. Redox peaks were not detected in the entire potential range (-0.5 - 0.5 Volts). Such feature is attributed to non-faradic process. Electrical double layer formation is predominant at electrode interfacial region. Electrical double layer formation is attributed to electrode polarization effect. In effect, electronic conduction is almost negligible during charge/discharge process [27].

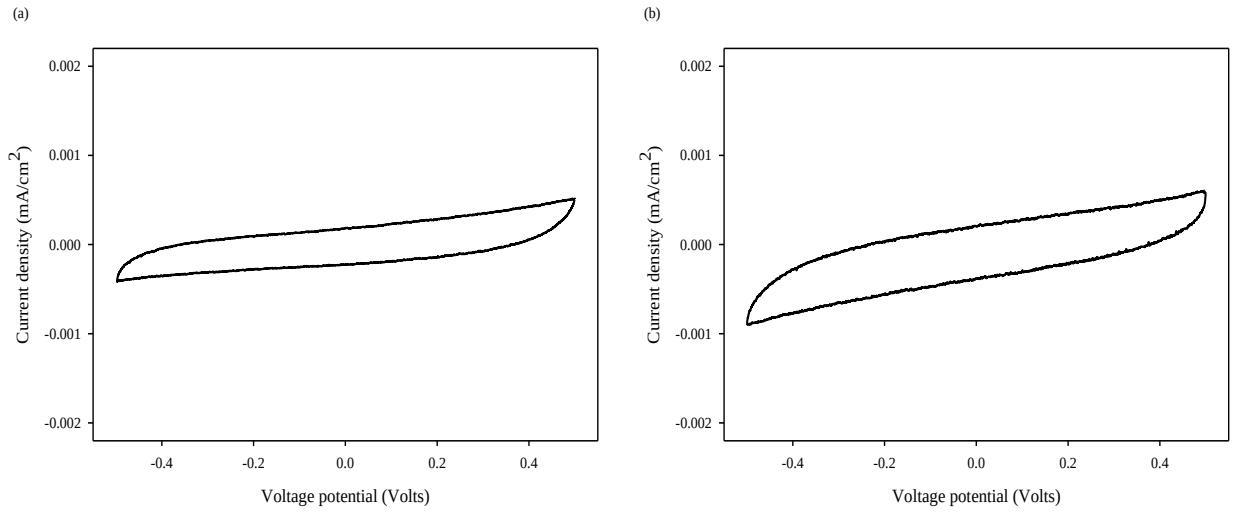

Figure 8. Cyclic voltammograms (a) MG49-25 wt.% $LiClO_4$ and (b) MG49-TiO_2-SiO_2-25 wt.% $LiClO_4$ polymer electrolyte

Broad coverage area was observed in MG49-TiO_2-SiO_2-$LiClO_4$ cyclic voltammogram. Broad coverage area is attributed to high current efficiencies. Such phenomenon is implicated to better electrochemical capacitance performance [28]. Reactive intercalation can result in large specific capacitance value. Reactive intercalation is attributed to high defect densities.

3.3 Morphological Analysis

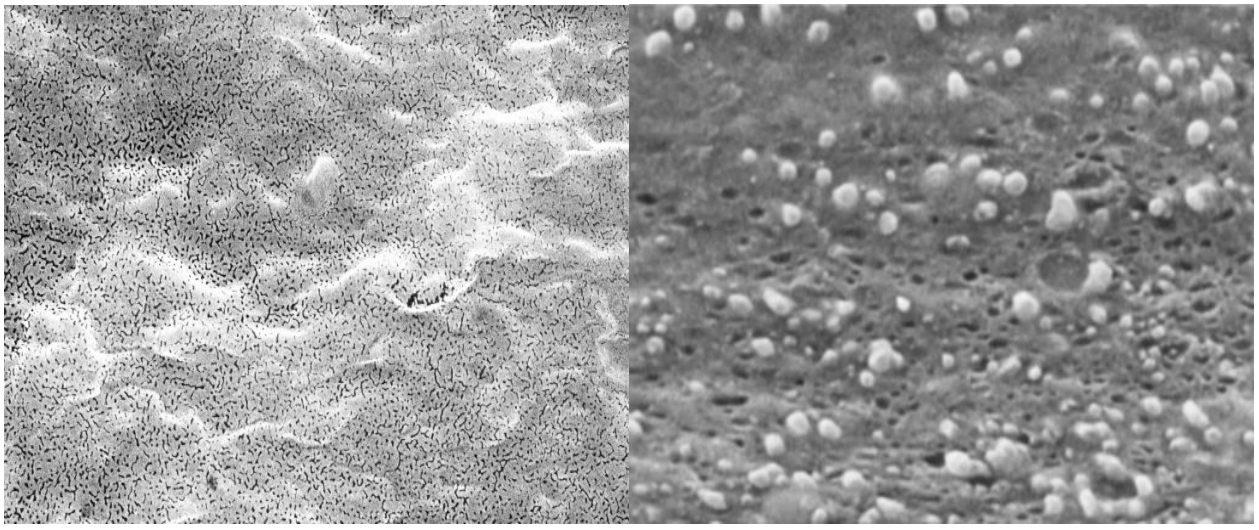

Figure 9. SEM images (a) MG49-25 wt.% $LiClO_4$ and (b) MG49-TiO_2-SiO_2-25 wt.% $LiClO_4$ polymer electrolyte

Uneven surface structure was observed in MG49-$LiClO_4$ polymer electrolyte. Irregular folded structure is attributed to polymer-salt complexation. Fine crack structure was observed in MG49-$LiClO_4$ polymer electrolyte. Fine crack structure is attributed to salt segreggation.

Spherulitic aggregate structure was observed in MG49-TiO_2-SiO_2-$LiClO_4$ polymer electrolyte. Such aggregate structure is discernable in uniform bright contrast. Spherulitic aggregate structure is attributed to TiO_2-SiO_2 agglomeration. Spherulitic aggregate particles might attach onto polymer chains. Spherulitic aggregate particles might reside at grain boundaries.

Continuous phase structure was observed in MG49-TiO_2-SiO_2-$LiClO_4$ polymer electrolyte. Continuous phase structure is attributed to crystallinity reduction. In most case, however, such phase structure is not present at stable equilibrium state.

Microscopic porous structure was observed in MG49-TiO_2-SiO_2-$LiClO_4$ polymer electrolyte. Such porous structure is attributed to solvent/non-solvent mutual diffusion. Microscopic porous structure can result in high electrochemical capacitive performance [29].

3.4 Thermal Analysis

Similar degradation patterns were observed in both polymer electrolytes. Such phenomenon is attributed to particle-polymer compatibility. Initial degradation stage was observed around 80 - 100 °C. Such degradation stage is attributed to solvent (or moisture) evaporation. No significant weight loss was observed prior to irreversible decomposition.

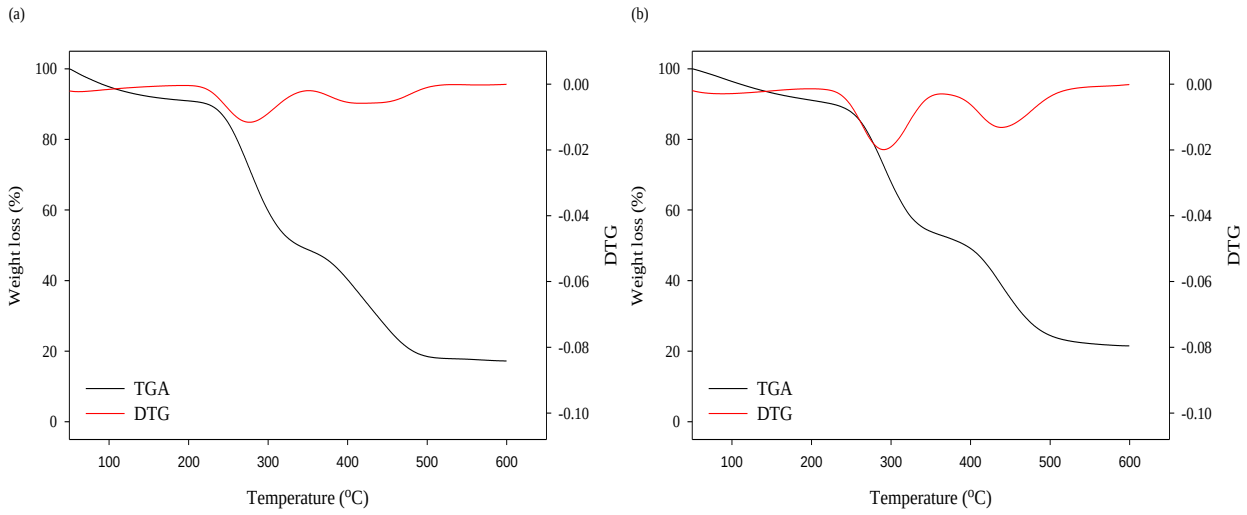

Figure 10. TGA thermograms (a) MG49-25 wt.% $LiClO_4$ and (b) MG49-TiO_2-SiO_2-25 wt.% $LiClO_4$ polymer electrolyte

In the present case, two distinct degradation phases were detected at high temperature region (as observed in DTG curves). Pronounced endothermic effect is attributed to thermal oxidative decomposition. First degradation step was observed around 270 - 290 °C. Such degradation step is attributed to $LiClO_4$ salt decomposition. Second degradation step was observed around 420 - 440 °C. Such degradation step is attributed to MG49 polymer chain decomposition. Transient degradation process is initiated at labile chain terminal. Such degradation process can occurs through random scission.

Onset degradation temperature was shifted upward upon TiO_2-SiO_2 reinforcement. Such phenomenon could contribute to stability enhancement. Intrinsic degradation mechanism is still not clear; however, such degradation behavior is most related to particle-polymer interaction.

3.5 Rheological Analysis

Strain sweep measurements were performed at a fixed angular frequency ω = 1 rad/s. Strain sweep profiles are presented in Figure 11. G′ and G″ were kept constant over small strain change; and then G′ and G″ had decreased above critical strain level. Such phenomenon is attributed to network deformation. In this case, G′ and G″ were strain independent up to 0.5% deformation amplitudes.

G′ and G″ had increased upon TiO_2-SiO_2 reinforcement. Such phenomenon is attributed to high deformation resistance. In fact, applied stress can prorogate through percolation mechanism. In general, applied stress is transferred across grain boundaries; and therefore, deformation energies are absorbed into TiO_2-SiO_2 nanoparticles.

G″ > G′ was observed in MG49-$LiClO_4$ polymer electrolyte. Such phenomenon is attributed to predominant viscous effect. Distinct behavior was observed in MG49-TiO_2-SiO_2-$LiClO_4$ polymer electrolyte. Distinct behavior is attributed to constituent interactions, i.e. particle-particle and/or particle-polymer interactions. In this case, therefore, rheological behavior is regulated through TiO_2-SiO_2 surface chemistry.

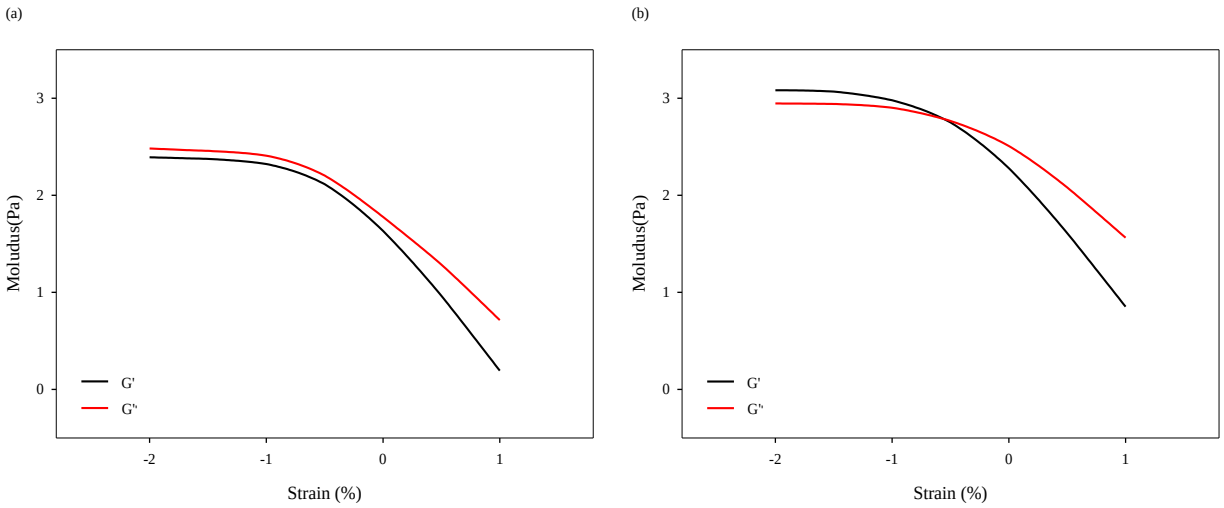

Figure 11. Strain sweep curves (a) MG49-25 wt.% $LiClO_4$ and (b) MG49-TiO_2-SiO_2-25 wt.% $LiClO_4$ polymer electrolyte

Frequency sweep measurements were performed at constant strain rate (0.5 %). Frequency sweep profiles are presented in Figure 12. Hyperbolic curve is obtained in the linear viscoelastic region. Small slope is attributed to better dispersion. Plateau modulus is observed at high angular frequencies. Plateau modulus is attributed to long-term relaxation behavior. Short-time dynamics are included at high angular frequencies. In effect, plateau modulus does not correlate to transient behavior [29].

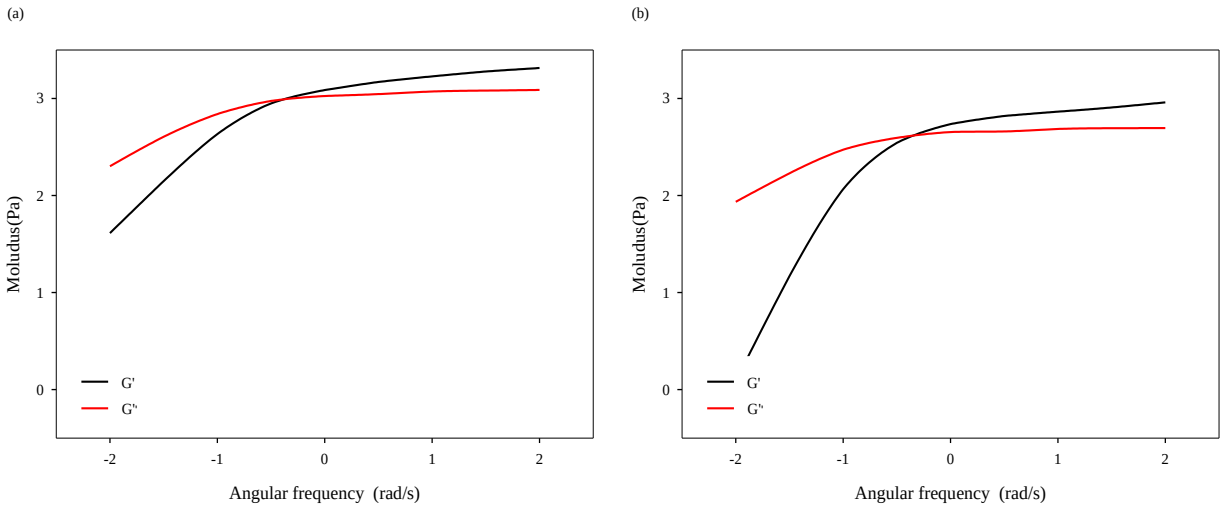

Figure 12. Frequency sweep curves (a) MG49-25 wt.% $LiClO_4$ and (b) MG49-TiO_2-SiO_2-25 wt.% $LiClO_4$ polymer electrolyte

G′/G″ was detected at moderate angular frequencies. In effect, G′ had become dominant at high angular frequencies (short time scales). G′/G″ is attributed to non-terminal relaxation behavior. In this case, however, crossover point did not change upon TiO_2-SiO_2 reinforcement.

G′ and G″ had reduced upon TiO_2-SiO_2 reinforcement. Such phenomenon is attributed to particle-polymer interaction [30]. G′ had a drastic increment at low angular frequencies. Such phenomenon is attributed to structural heterogeneities.

4. CONCLUSION

In the present investigation, MG49-TiO_2-SiO_2-$LiClO_4$ polymer electrolyte had exhibited maximum ionic conduction as 6.95×10^{-07} S/cm. MG49-TiO_2-SiO_2-$LiClO_4$ polymer electrolyte can provide stable operation over a broad operational range.

ACKNOWLEDGEMENT
Authors would like to acknowledge financial support from research grant: (1) NND/NM (2)/TD11-046 and (2) ERGS/1/2013/TK07/UKM/02/4. Authors would also like to acknowledge technical support from CRIM.

References

1. D.K. Pradhan, R.N.P. Choudhary, B.K. Samantaray, *Int. J. Electrochem. Sci.* 3 (2008) 597.
2. H.H. Sumathipala, J. Hassoun, S. Panero, B. Scrosati, *Ionics* 13 (2007) 281.
3. S. Ibrahim, M.R. Johan, *Int. J. Electrochem. Sci.* 7 (2012) 2596.
4. S. Neelam, K. Manindra, *Solid state Ionics* 262 (2014) 806.
5. P.C. Sekhar, P.N. Kumar, A.K. Sharma, *J. Appl. Phys.* 2 (2012) 1.
6. S. Rajendran, M. Sivakumar, R. Subadevi, *Mater. Lett.* 58 (2004) 641.

7. S.K. Tripathi, A. Gupta, A. Jain, M. Kumari, *Indian J. Pure Appl. Phys.* 51 (2013) 358.
8. A.S. Shaplov, R. Marcilla, D. Mecerreyes, *Electrochim. Acta* 175 (2015) 18.
9. Y.L. Yap, A.H. You, L.L. Teo, H. Hanapei, *Int. J. Electrochem. Sci.* 8 (2013) 2154.
10. N. Shukla, A.K. Thakur, A. Shukla, D.T. Marx, *Int. J. Electrochem. Sci*. 9 (2014) 7644.
11. B. Smitha, S. Sridhar, A.A. Khan, *J. Membr. Sci*. 259 (2005) 10.
12. K.S. Ji, H.S. Moon, J.W. Kim, J.W. Park, *J. Power Sources* 117 (2003) 124.
13. A.L. Saroj, R.K. Singh, *J. Phys. Chem. Solids* 73 (2012) 162.
14. H. Suhermana, A.B. Sulonga, J. Sahari, *Ceram. Int*. 39 (2013) 1277.
15. C. Tang, K. Hackenberg, Q. Fu, P.M. Ajayan, H. Ardebili, *Nano Lett.* 12 (2012) 1152.
16. D. Ling, W. Liu, Y. Liu, H.R. Lee, P. Hsu, K. Liu, Y. Cui, *Nano Lett.* 16 (2016) 459.
17. S.H. Kim, J.Y. Kim, H.S. Kim, H.N. Cho, *Solid State Ionics* 116 (1999) 63.
18. A. Ahmad, C.L. Pow, M.S. Suait, *Sains Malays*. 39 (2010) 65.
19. J.D. Jeon, S.Y. Kwak, B.W. Cho, *J. Electrochem. Soc*. 152 (2005) 1583.
20. D.K. Cha, S.M. Park, *J. Electroanal. Chem*. 459 (1998) 135.
21. S.K. Deraman, N.S. Mohamed, R.H.Y. Subban, *Int. J. Electrochem. Sci.* 8 (2013) 1459.
22. L.C. Rodrigues, P.C. Barbosa, M.M. Silva, M.J. Smith, *Electrochim. Acta* 53 (2007) 1427.
23. H.M. Kao, C.L. Chen, S.W. Chiao, *J. Chin. Chem. Soc.* 52 (2005) 693.
24. M.G. McLin, C.A. Angell, *J. Phys. Chem*. 6 (1991) 9464.
25. K. Pandey, M.M. Dwivedi, N. Asthana, M. Singh, S.L. Agrawal, *Mater. Sci. Appl.* 2 (2011) 721.
26. P. Judeinstein, D. Reichert, E.R. Azevedo, T.J. Bonagamba, *Acta Chim. Slov.* 52 (2005) 349.
27. C. Liew, S. Ramesh, *Materials* 7 (2014) 4019
28. C.S. Lim, K.H. Teoh, C.W. Liew, S. Ramesh, *Ionics* 20 (2014) 251.
29. D. Ravindrani, P. Vickraman, *Chem. Sci. Trans.* 4 (2015) 373.
30. S.R. Raghavan, M.W. Riley, P.S. Fedkiw, S.A. Khan, *Chem. Mater.* 10 (1998) 244.